Research Article

Chalcones Derived from 2-Acetylpyrrole and Their Co(II), Ru(III) Structural Analysis Complexes: Docking research and anti-lung cancer activity (A549)

Rusul B. Fadhil[1], Jasim M.S. Alshawi[1]*

[1]Department of Chemistry, College of Education for Pure Sciences, University of Basrah, Basrah 61001, Iraq.

*Corresponding Author: Jasim M.S. Alshawi , jasim.salih@uobasrah.edu.iq

ABSTRACT

In the present study, synthesis and characterization of a new chalcons derived from 2-Acetylpyrrole and three other aldehydes as well as its uninuclear complexes including Co(II), and Ru(III) is reported. The ligand and its metal complexes have been characterized by FTIR, 1H NMR, 13C NMR, UV-Vis spectrophotometry, mass spectrometry, molar conductance, magnetic susceptibility, and thermal gravimetric analysis. Spectroscopic and physicochemical results confirmed coordination through the carbonyle and nitrogen atom of pyrrole and indicated the proposed Tetrahedral coordination geometry,. Anticancer activity of the synthesized Chalcones and its metal complexes has been examined against Lung cancer (A549) by MTT method. All compounds exhibited dose-dependent anticancer activity, and the ^{1}L ligand with its complex of Co(II) show exhibited inhibitory activity against cancer cells while showing lower toxicity toward normal cells at a concentration of 1 mM. The study were confirmed by docking study.

Keywords: chalcones, Tetrahedral, Anticancer, docking, Lung cancer.

INTRODUCTION

Beyond biomedical research, the structural diversity and functional versatility of chalcone-based complexes have attracted interest in industrial, agricultural, and environmental applications[1, 2]. Their potential anticancer properties, however, represent an important area of investigation, particularly in response to the continuing global burden of cancer[3–5] . Despite advances in chemotherapy and targeted treatment, therapeutic resistance, tumor heterogeneity, recurrence, and metastasis remain major obstacles to successful cancer management[6–8] . These challenges highlight the need to identify alternative molecular structures with promising biological activities. Chalcone derivatives and their metal complexes have therefore received increasing attention because modifications to the chalcone framework and coordination with metal ions may influence their physicochemical characteristics and interactions with cellular targets[9–12]

Lung cancer remains a major cause of cancer-related mortality[13] , with non-small cell lung cancer (NSCLC) accounting for approximately 80–90% of lung cancer cases[14, 15] .Its progression involves dysregulated cellular proliferation, impaired apoptosis, invasion, and metastatic spread. Angiogenesis is another critical process, enabling tumors to establish new blood vessels that supply oxygen and nutrients and facilitate further growth and dissemination[16, 17] .

The vascular endothelial growth factor (VEGF) and vascular endothelial growth factor receptor-2 (VEGFR-2) signaling pathway is a central regulator of tumor-associated angiogenesis[18–20] .Receptor activation initiates intracellular signaling events that stimulate endothelial-cell proliferation, migration, and survival, thereby supporting vascular development within the tumor microenvironment. Consequently, targeting VEGF/VEGFR-2 signaling represents a potential strategy for restricting angiogenesis and tumor progression.

In this context, chalcone-based compounds provide a promising chemical platform for investigating potential anticancer agents. Metal coordination may further modify ligand properties and influence biological interactions. Accordingly, evaluating chalcone derivatives and their metal complexes against angiogenesis-related targets, particularly VEGFR-2, may contribute to the identification of candidate compounds for future NSCLC research. Combining coordination chemistry with molecular docking and experimental biological evaluation could provide complementary evidence regarding their potential mechanisms of action and therapeutic relevance[21] .

Materials and methods:

Materials and Instrumentation

All chemical reagents used for this experiment were of analytical purity and were supplied by Merck company without further purification. The experiments were carried out in the Department of Chemistry, University of Basrah. The melting point of all synthesized compounds was measured using a melting point device produced by Thermo Fisher Scientific. Reaction progress was monitored by TLC on silica gel plates.

The IR spectra of the samples were recorded over 400-4000 cm^{-1} using a Shimadzu FTIR-8400S spectrometer with KBr pellets. Proton nuclear magnetic resonance spectroscopy (^{1}H NMR) was recorded on a Bruker 400 MHz NMR spectrometer in

deuterated dimethyl sulfoxide (DMSO-d_6). The molar conductivity was determined in DMF solution using in 10^{-3}M (conc.) (25 C) a Jenway PCMB conductivity meter. UV–Vis spectra were recorded in ETOH using an SPV-725 spectrophotometer.
The metal-to-ligand ratio was determined using an atomic absorption spectrophotometer (Analyst 200). The magnetic susceptibility at room temperature was determined by the Gouy method using an automatic susceptibility balance manufactured by Sherwood Scientific at the Department of Chemistry, Al-Mustansiriya University, Baghdad.
Electrospray ionization mass spectra (ESI-MS) were recorded in acetonitrile using a Waters Alliance HPLC system coupled with a Quattro micro-API mass spectrometer in Tehran, Iran.

Synthesis of the Chalcones Ligand

The chalcone ^{1}L was synthesized via a 1:1 molar condensation of 3-phenoxybenzaldehyde (1mmol,0.198 g) and 2-acetylpyrrole (1mmol, 0.109 g) in 10 mL of absolute ethanol using KOH (0.30 g) as the base. The reaction mixture was sonicated at 60 °C for 1 h, and the reaction progress was monitored by TLC. After completion, the mixture was cooled with ice and acidified gradually with glacial acetic acid to pH= 6. The precipitated product was filtered, dried, and recrystallized from ethanol to afford the purified chalcone.. The structure of the synthesized ligand is given in Fig.1. Its physical properties are shown in Table 1[22, 23] .
The synthesized chalcone ligand was obtained as an orange crystalline solid in 80% yield, with a melting point of 121–123 °C. The ^{1}H NMR spectrum (DMSO-d_6, 400 MHz, δ ppm) confirmed the structural features of the ligand, showing a characteristic singlet at δ ≈ 12.02 ppm assigned to proton (NH,1H), and the doublet single at 7.03ppm is attributed to(1H,6) CH=CH (J=15.7Hz) while the single at (7.75ppm) belong to(1H,7) CH=CH (J=7.8Hz), along with multiple signals in the region δ 6.27-7.71ppm corresponding to aromatic protons (12H). The ^{13}C NMR spectrum (DMSO-d_6) displayed signals in the range δ 110.69-157.30ppm(16C,Ar), attributed to the aromatic carbons, the single at ((118.79,140.37ppm for (C_6 =C_7), and the single at (178.08ppm) belong to (C5, C═O).
The FTIR spectrum (ν, cm^{-1}) exhibited characteristic absorption bands at 2956 cm^{-1} (aliphatic C–H), 3118 cm^{-1} (aromatic C–H), 3277cm^{-1} (NH), 1647cm^{-1} (C=O stretching), 1581 cm^{-1} (chalcone C=C), and 1159 cm^{-1} (C–N), confirming the formation of the chalcone linkage (Table 2) [24] .
The UV–Vis spectrum showed a prominent absorption band at 299 nm, attributed to π→π* electronic transitions within the conjugated system (Figure 7).
Mass spectrometric analysis revealed a molecular ion peak at m/z = 289.90, corresponding to the expected molecular weight of the ligand and consistent with the base peak, further confirming its structure[25] .
Chalcones ^{2}L and ^{3}L, namely 3-(7-methoxynaphthalen-2-yl)-1-(1H-pyrrol-2-yl)prop-2-en-1-one and 3-[4-(benzyloxy)-3-methoxyphenyl]-1-(1H-pyrrol-2-yl)prop-2-en-1-one, respectively, were synthesized following the same procedure described above. 2-Acetylpyrrole (1mmol, 0.109 g) was reacted with 6-methoxy-2-naphthaldehyde (1mmol, 0.186 g) for ^{2}L and 3-benzyloxy-4-methoxybenzaldehyde (1mmol, 0.242 g) for ^{3}L, using ethanol as the solvent. The products were obtained in 70-85% yield with a melting point (^{2}L) of 233–235°C,(^{3}L) 135-137°C.
The ^{1}H NMR spectrum (DMSO-d_6, 400 MHz, δ ppm) confirmed the structural features of the ligand(^{2}L), showing a characteristic singlet at δ ≈ 12.04 ppm assigned to proton (NH,1H), and the doublet single at 7.18ppm is attributed to(1H,6) CH=CH (J=20.2Hz) while the single at (7.89ppm) belong to(1H,7) CH=CH
(J=8.8Hz), along with multiplet signals in the region δ 6.29-8.21ppm corresponding to aromatic protons (9H)[26] .
The ^{13}C NMR spectrum (DMSO-d_6) displayed signals in the range δ 106.73-158.80ppm(14C,Ar), attributed to the aromatic carbons, the single at(55.78ppm)for (OCH_3),the single at (119.64, 141.45ppm) for (C6 =C7), and the single at (178.29ppm) belong to (C_5, C═O).
The FTIR spectrum (ν, cm^{-1}) exhibited characteristic absorption bands at 2966cm^{-1} (aliphatic C–H), 3115 cm^{-1} (aromatic C–H), 3225cm^{-1} (NH), 1643cm^{-1} (C=O stretching), 1579 cm^{-1} (chalcone C=C), and 1178cm^{-1} (C–N), confirming the formation of the chalcone linkage (Table 2).
The UV–Vis spectrum showed a prominent absorption two bands at 261 and 372 nm, attributed to π→π* electronic transitions within the conjugated system (Figure8,).
Mass spectrometric analysis revealed a molecular ion peak at m/z 277.90, corresponding to the expected molecular weight of the ligand and consistent with the base peak, further confirming its structure.
The ^{1}H NMR spectrum (DMSO-d_6, 400 MHz, δ ppm) confirmed the structural features of the ligand(^{3}L), showing a characteristic singlet at δ ≈ 11.99ppm assigned to proton (NH,1H), the singlet at single 3.84ppm(s,1H,OCH_3), 5.22ppm(s,1H,CH_2),and the doublet single at 7.15ppm is attributed to(1H,6) CH=CH
(J=16Hz) while the single at (7.60ppm) belong to(1H,7) CH=CH (J=12Hz), along with multiple signals in the region δ 7.09-7.50ppm corresponding to aromatic protons (11H). The ^{13}C NMR spectrum (DMSO-d_6) displayed signals in the range δ 110.44-150.20ppm(16C,Ar), attributed to the aromatic carbons, the single at(56.25ppm)for (OCH3), the single at 70.48ppm for(C14)(CH_2), the single at (121.38, 141.44ppm) for (C_6 =C_7), and the single at (178.39ppm) belong to (C_5, C═O).
The FTIR spectrum (ν, cm^{-1}) exhibited characteristic absorption bands at 2952cm^{-1} (aliphatic C–H), 3090 cm^{-1} (aromatic C–H), 3232cm^{-1} (NH), 1645cm^{-1} (C=O stretching), 1581 cm^{-1} (chalcone C=C), and 1271cm^{-1} (C–N), confirming the formation of the chalcone linkage (Table 2)[27] .
The UV–Vis spectrum showed a prominent absorption band at 295 nm, attributed to π→π* electronic transitions within the conjugated system (Figure 9).

Mass spectrometric analysis revealed a molecular ion peak at m/z 333.90, corresponding to the expected molecular weight of the ligand and consistent with the base peak, further confirming its structure.

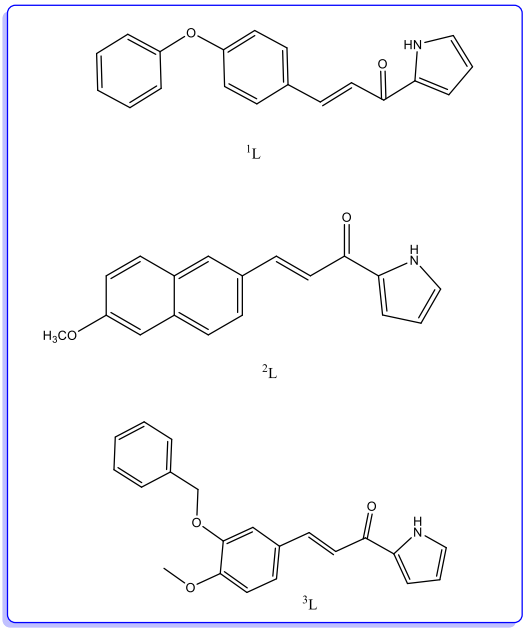


Figure 1. The chemical structure of the Chalcones.

Synthesis of Metal Complexes

The ruthenium complex was prepared using a 2:1 molar ratio of chalcone ligand ^{1}L to $RuCl_3$. Chalcone ^{1}L (2mmol, 0.578 g) and $RuCl_3$ (1mmol, 0.207g) were dissolved in a solvent mixture of EtOH/MeOH/DMF (4:4:2). The reaction mixture was sonicated at 60 °C for 2 h, yielding a dark-green precipitate. The precipitate was collected by filtration and washed several times with diethylether .Table 1and Figure2 [28–30].

The ruthenium complex (^1L_2Ru) was obtained as a uninuclear dark green crystalline solid in 47% yield, with a melting point above >300 °C. Mass spectrometric analysis showed a base peak at m/z ≈ 277 and a molecular ion peak at m/z 678 [M+2], consistent with the proposed structure Figure 6. The FTIR. spectrum (ν, cm^{-1}) exhibited characteristic bands at 2934 (aliphatic C–H), 3075 (aromatic C–H), 1627 (C=O), 1580 (chalcone C=C), 1181 (C–N), and 515cm^{-1} assigned to M–N stretching vibrations, confirming coordination through the pyrrole nitrogen and carbonyl oxygen atoms Figure 4) [31] . The UV–Vis spectrum showed two absorption bands at 284 nm\388 (π→π*) and at 600 nm corresponding to d–d transitions Figure 7.

The ruthenium complexes of chalcones ^2L_2Ru and ^3L_2Ru were prepared separately following the procedure described above, using a 2:1 molar ratio of ligand to metal salt. $RuCl_3$ (1mmol, 0.207 g) was reacted with ^{2}L (2mmol, 0.554 g) and ^{3}L (2mmol, 0.666 g) separately. The reactants were dissolved in a solvent mixture of EtOH/MeOH/DMF (4:4:2) and subjected to ultrasonic irradiation for 2 h. Dark-green precipitates were formed, which were collected by filtration and washed several times with diethyl ether[32] .

The ruthenium complexes (^2L_2Ru) was isolated as an dark green solid in 45% yield, with a melting point exceeding >300 °C. Its mass spectrum displayed a base peak at m/z =616 and a molecular ion peak at m/z 654 [M+1]. Figure 6. The FTIR spectrum showed bands at 2929 (aliphatic C–H), 3040 (aromatic C–H), 1626 (C=O), 1570 (chalcone C=C), 1109 (C–N), and 431 cm^{-1} (M–N) Figure 4. The UV–Vis spectrum exhibited two absorption bands at 290 nm\368nm (π→π*) and at 725 nm attributed to d–d transitions Figure 8.

The ruthenium complexes (^3L_2Ru) was obtained as a dark green solid in 53% yield, with a melting point above >300 °C. Mass spectrometric analysis showed a base peak at m/z = 182 and a molecular ion peak at m/z = 865.20 [M]. Figure 6. The FTIR spectrum (ν, cm^{-1}) displayed bands at 2932 (aliphatic C–H), 3072 (aromatic C–H), 1622 (C=O), 1596 (aromatic C=C), 1044 (C–N), and 521 cm^{-1} (M–N). Figure 4. The UV–Vis spectrum showed absorption bands at 271 nm (π→π*) and 692 nm\733nm corresponding to d–d transitions Figure 9.

The cobalt(II) complexes of chalcones ^1L_2Co–^3L_2Co were synthesized separately using a 2:1 molar ratio of ligand to metal salt. Each chalcone, ^{1}L (2mmol, 0.578 g), ^{2}L (2mmol, 0.554 g), and ^{3}L (2mmol, 0.666 g), was reacted separately with $CoCl_2{\cdot}6H_2O$ (1mmol, 0.237 g) in a solvent mixture of EtOH/MeOH/DMF (4:4:2). The reaction mixtures were subjected to ultrasonic irradiation at 60 °C for 2 h, resulting in the formation of dark-yellow to yellow precipitates. The products were collected by filtration and washed several times with diethyl ether.

The cobalt(II) complexes (^1L_2Co) was obtained as a dark yellow solid in 50% yield, with a melting point above >300 °C. The mass spectrum revealed a base peak at m/z = 290 and a molecular ion peak at m/z = 637$[M+2]^+$Figure 6. The FTIR spectrum (ν, cm^{-1}) showed bands at 2950 (aliphatic C–H), 3050 (aromatic C–H), 1640 (C=O), 1576 (aromatic C=C), 1159 (C–N), and 527-

cm^{-1} (M–N). Figure 4. The UV–Vis spectrum exhibited absorption bands at 346nm (π→π*) and at 568 nm\730 assigned to d–d transitions Figure 7.

The cobalt(II) complexes ($^{2}L_2Co$) was obtained as a pale yellow solid in 48% yield, with a melting point above >300 °C. The mass spectrum revealed a base peak at m/z = 277and a molecular ion peak at m/z = 613$[M+2]^{+}$Figure 6. The FTIR spectrum (ν, cm^{-1}) showed bands at 2965 (aliphatic C–H), 3071 (aromatic C–H), 1636 (C=O), 1577 (chalcone C=C), 1183 (C–N), and 478cm^{-1} (M–N). Figure 4. The UV–Vis spectrum exhibited two absorption bands at 260nm and 342 nm (π→π*) and at 733nm assigned to d–d transitions Figure 8.

The cobalt(II) complexes ($^{3}L_2Co$) was obtained as a orange solid in 58% yield, with a melting point above >300 °C. The mass spectrum revealed a base peak at m/z = 115and a molecular ion peak at m/z = 725$[M+2]^{+}$Figure 6. The FTIR spectrum (ν, cm^{-1}) showed bands at 2931 (aliphatic C–H), 3070 (aromatic C–H), 1629 (C=O), 1579 (chalcone C=C), 1124 (C–N), and 560cm^{-1} (M–N). Figure 4. The UV–Vis spectrum exhibited absorption bands at 297 nm (π→π*) and at 741nm \ 766 nm assigned to d–d transitions Figure 9

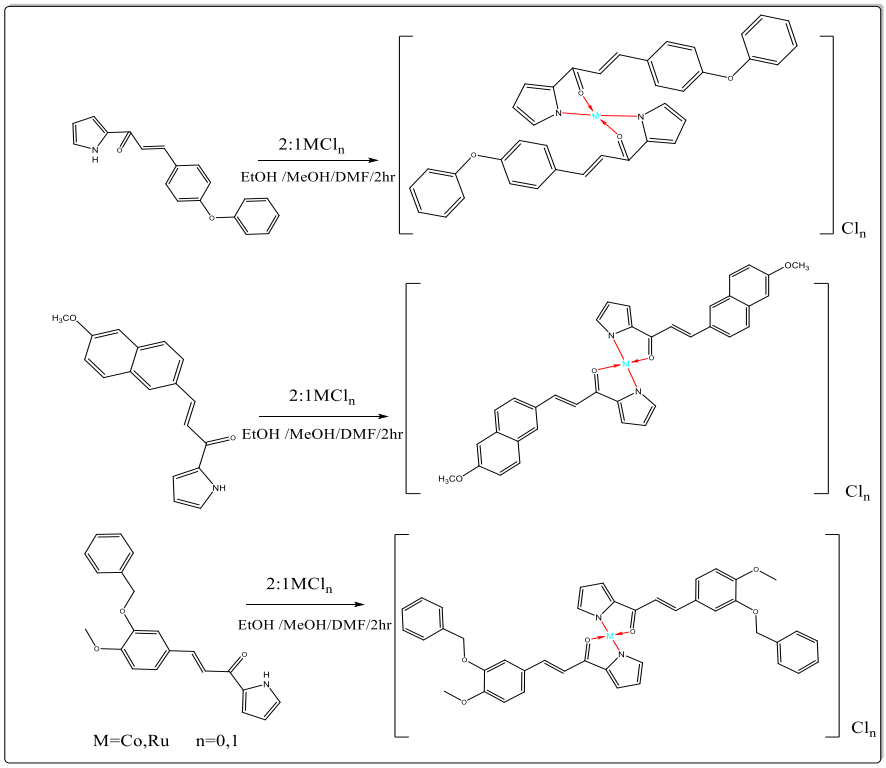


Figure 2: Characteristics of complexes and ligands.

Table 1:Phesical properties of Ligands and there complexes

Comp. No.	M.F	Colour	M.Wt g/mole	M.P.	Yield %
^{1}L	$C_{19}H_{15}NO_2$	Yellowish white	289.33	121-123	**80**
$^{1}L_2Ru$	$[Ru(C_{38}H_{30}N_2O_4)]Cl$	Dark green	713.17	>300	**47**
$^{1}L_2Co$	$[Co(C_{38}H_{30}N_2O_4)]$	Dark yellow	635.59	>300	**50**
^{2}L	$C_{18}H_{15}NO_2$	Dark yellow	277.32	233-235	**85**
$^{2}L_2Ru$	$[Ru(C_{36}H_{30}N_2O_4)]Cl$	Dark green	689.15	>300	**45**
$^{2}L_2Co$	$[Co(C_{36}H_{30}N_2O_4)]$	Pale yellow	611.56	>300	**48**

^{3}L	$C_{21}H_{19}NO_3$	Pale yellow	333.39	135-137	**70**
^{3}L$_2$Ru L	[Ru($C_{42}H_{38}N_2O_6$)]Cl	Dark green	801.28	>300	**53**
^{3}L$_2$Co	[Co($C_{42}H_{38}N_2O_6$)]	Orange	723.69	>300	**58**

Results and Discussions:

The three chalcone ligands were successfully prepared through the condensation reaction between 3-phenoxybenzaldehyde, 6-methoxy-2-naphthaldehyde, and 3-benzyloxy-4-methoxybenzaldehyde with 2-acetylpyrrole using an ultrasonic procedure. Formation of the chalcone ligands was evidenced by the incorporation of the α,β-unsaturated carbonyl group, as revealed by FTIR and NMR spectroscopy techniques. For instance, in FTIR, the disappearance of the aldehyde carbonyl stretching band and the appearance of the characteristic conjugated C=O bond stretch at about 1600 cm^{-1} and C=C bond stretch at about 1500 cm^{-1} On the other hand, observation of the characteristic olefinic proton signals of the α,β-unsaturated system in the ^{1}H NMR spectra, which appeared in the range of δ = 7.03–7.89 ppm, also suggests the formation of the chalcone ligands Following complexation with metal ions such as Co(II) and Ru(III), significant changes were observed in their spectra, suggesting the formation of metal–ligand complexes. In particular, the FTIR spectra of the complexes showed a decrease in the absorption frequency of the carbonyl (C=O) band, implying the participation of the oxygen atom in the complex formation. In addition, the presence of new bands around 431–560cm^{-1}, which can be attributed to M–O and M–N vibrations, confirms the participation of both the carbonyl oxygen and pyrrole nitrogen atoms in coordination.

The results of mass spectrometry provide compelling proof that binuclear complexes have been formed, as indicated by molecular ion peaks matching those predicted based on molecular weights. The match between observed and theoretical m/z ratios confirms the composition of the complexes.

Table 2: The FTIR spectral data (cm^{-1}) of the synthesized chalcones ligand and its corresponding metal complexes are presented and discussed.

Sym.	NH	υC=H (Alipha.)	υC=H(Ar.)	υC=O	υC=C(Ch.)	υC-N	M-N
^{1}L	3277	2956	3118	1647	1581	1159	-
^{1}L$_2$Ru		2934	3075	1627	1580	1181	515
^{1}L$_2$Co		2950	3050	1640	1576	1159	527
^{2}L	3225	2966	3115	1643	1579	1178	
^{2}L$_2$Ru		2929	3040	1626	1570	1109	431
^{2}L$_2$Co		2965	3071	1636	1577	1183	478
^{3}L	3232	2952	3090	1645	1581	1271	
^{3}L$_2$Ru		2932	3072	1622	1596	1044	521
^{3}L$_2$Co		2931	3070	1629	1579	1124	560

Conductivity and Magnetic Properties

The molar conductivities(Λm) of the synthesized Ru(III) and Co(II) complexes ranged from 23 to 55 $S\cdot cm^2\cdot mol^{-1}$ in DMF at a concentration of 1×10^{-3} M and at room temperature (Table 3). The Ru(III) complexes exhibited electrolytic behavior, indicating the presence of chloride ions outside the coordination sphere. These chloride ions act as counterions and dissociate in DMF solution, resulting in increased ionic mobility and higher molar conductivity. In contrast, the Co(II) complexes showed non-electrolytic behavior, indicating the absence of chloride ions outside the coordination sphere.[33, 34]

The magnetic susceptibility measurements provided further information about the electronic configurations and geometries of the synthesized complexes. The Ru(III) and Co(II) ions possess (d^5) and (d^7) electronic configurations, respectively. Their magnetic behavior is attributed to the presence of unpaired electrons in the (d)-orbitals. Based on the magnetic susceptibility measurements and the spectroscopic data, the synthesized Ru(III) and Co(II) complexes are proposed to adopt tetrahedral geometries. [35, 36]

The effective magnetic moments (μ_eff), calculated using standard equations, agree with the proposed coordination modes and further support the suggested geometries of the complexes.

$$xm = xg * M.wt \ldots\ldots\ldots 1$$
$$xA = xm + D \ldots\ldots\ldots 2$$
$$\mu eff = 2.828\sqrt{(XA * T\,B.M} \ldots\ldots\ldots 3$$

Electronic Spectra (UV–Vis Analysis)

Electronic absorption spectra of the three chalcone ligands (^{1}L, ^{2}L, and ^{3}L) and the metal complexes were recorded in DMSO. Table 3 and Figure 6 present the results. The electronic absorption spectra provide detailed information on electronic transitions and the metal ions' coordination environment. The free ligands (^{1}L, ^{2}L, and ^{3}L) exhibited intense absorption bands at 299,(261, 372), and 295 nm, respectively, attributed to π→π* electronic transitions in the aromatic system and the α,β-unsaturated carbonyl moiety (-CH=CH-C=O). The presence of these absorption bands verifies that conjugation occurs in the ligand structures[37] .

Regarding ligand–metal interactions, changes in the electronic spectra were observed, indicating successful complexation. Intra-ligand transitions (π→π*)occurred in the ultraviolet region, while (d-d) transitions appeared in the visible region. The Ru(III) complex(^1L_2Ru) showed two absorption bands at 284 and 388 nm, attributed to a (π→π*) transition, while the absorption band at 600 nm was assigned to a (d-d) transition ($^6A_1 \rightarrow {}^4T_1$). For the tetrahedral Ru(III) complex with a (d^5) configuration, this transition can be assigned to the spin-forbidden transition from the($^6A_1$) ground state to an excited ($^4T_1$) state.

The Co(II) complex(^1L_2Co) showed two absorption bands at 260 and 342 nm due to a π→π* transition, while the absorption bands at 568 and 730 nm were attributed to (d-d) transitions. For the tetrahedral Co(II) complex with a (d^7) configuration, these transitions can be assigned to ($^4A_2 \rightarrow {}^4T_2$)and ($^4A_2 \rightarrow {}^4T_1$), respectively. The observed electronic spectra are consistent with a tetrahedral geometry around the metal ions[38] .

Regarding ligand–metal interactions, changes in the electronic spectra were observed, indicating successful complexation. Intra-ligand transitions (π→π*) occurred in the ultraviolet region, while (d-d) transitions appeared in the visible region. The Ru(III) complex(^2L_2Ru) showed two absorption bands at 290 and 368 nm, attributed to a (π→π*) transition, while the absorption band at 725 nm was assigned to a (d-d) transition ($^6A_1 \rightarrow {}^4T_1$). For the tetrahedral Ru(III) complex with a (d^5) configuration, this transition can be assigned to the spin-forbidden transition from the($^6A_1$) ground state to an excited ($^4T_1$) state.

The Co(II) complex(^2L_2Co) showed an absorption band at 346 nm due to a π→π* transition, while the absorption band at 733 nm were attributed to (d-d) transitions. For the tetrahedral Co(II) complex with a (d^7) configuration, these transitions can be assigned to ($^4A_2 \rightarrow {}^4T_2$), respectively. The observed electronic spectra are consistent with a tetrahedral geometry around the metal ions[39] .

Regarding ligand–metal interactions, changes in the electronic spectra were observed, indicating successful complexation. Intra-ligand transitions (π→π*)occurred in the ultraviolet region, while (d-d) transitions appeared in the visible region. The Ru(III) complex(^3L_2Ru) showed an absorption band at 271 nm, attributed to a (π→π*) transition, while the absorption bands at 692 and 733 nm was assigned to a (d-d) transition ($^6A_1 \rightarrow {}^4T_1$) and ($^6A_1 \rightarrow {}^4T_2$) . For the tetrahedral Ru(III) complex with a (d^5) configuration, this transition can be assigned to the spin-forbidden transition from the($^6A_1$) ground state to an excited ($^4T_1$) state.

The Co(II) complex(^3L_2Co) showed an absorption band at 297 nm due to a π→π* transition, while the absorption bands at 741 and 766 nm were attributed to (d-d) transitions. For the tetrahedral Co(II) complex with a (d^7) configuration, these transitions can be assigned to ($^4A_2 \rightarrow {}^4T_2$)and ($^4A_2 \rightarrow {}^4T_1$), respectively. The observed electronic spectra are consistent with a tetrahedral geometry around the metal ions.[40]

Table 3: Electronic Spectral Data, Molar Conductance, and Magnetic Moments of the Ligand and Its Metal Complexes

Compound	λmax (nm)	ε (L·mol^{-1}·cm^{-1})	Assignment	Λ_m (S·cm^2·mol^{-1})	μeff (B.M.)
^{1}L(Ligand)	299	154000	π → π*	----	----
^1L_2Co	346	96000	π → π*	25	3.35
	568	2500	d–d ($^4A_2 \rightarrow {}^4T_2$)		
	730	2000	d–d($^4A_2 \rightarrow {}^4T_1$)		
^1L_2Ru	284 388	64000 97000	π → π*	75	5.66
	600	2400	d–d ($^6A_1 \rightarrow {}^4T_1$)		

Compound	λmax (nm)	ε (L·mol^{-1}·cm^{-1})	Assignment	Λ_m (S·cm^2·mol^{-1})	μeff (B.M.)
^{2}L	261 372	152000 170000	π → π*	----	----
^{2}L$_2$Co	260 342	19500 100000	π → π*	23	3.27
	733	13700	d–d (^{4}A$_2$→^{4}T$_2$)		
^{2}L$_2$Ru	290 368	58000 48000	π → π*	84	5.67
	725	1900	d–d (^{6}A$_1$→^{4}T$_1$)		
^{3}L	295	181000	π → π*	----	----
^{3}L$_2$Co	297	91000	π → π*	26	3.72
	741	2531	d–d (^{4}A$_2$→^{4}T$_2$)		
	766	2130	d–d(^{4}A$_2$→^{4}T$_1$)		
^{3}L$_2$Ru	271	117000	π → π*	76	5.89
	692	2451	d–d (^{6}A$_1$→^{4}T$_1$)		
	733	2000	d–d (^{6}A$_1$→^{4}T$_2$)		

Thermogravimetric analysis (TGA)

The TGA of the synthesized complexes was performed under nitrogen using a simultaneous thermal analyzer with a heating rate of 10 °C/min from room temperature to 600 °C (Table 4 and Figure 10). The thermal data obtained will be helpful in understanding the stability of the complexes[41–43].

The TGA curve of the ^{1}L$_2$Ru complex indicates high thermal stability, with no significant mass loss observed below 120 °C. The complex undergoes a single-step decomposition over the temperature range of 120–600 °C, corresponding to the loss of $C_{13}H_{17}O$ N Cl, with an experimental mass loss of 33.47%, in good agreement with the calculated value.

The TGA results of the ^{1}L$_2$Co complex indicate high thermal stability, with no appreciable mass loss below 100 °C. The thermal decomposition occurs in two successive steps. The first step takes place over 100–270 °C, corresponding to the loss of C_3H_7N, with a theoretical mass loss of 8.99%. The second step occurs over 270–600 °C, corresponding to the loss of $C_{11}H_{12}O_2N$, with theoretical and experimental mass losses of 29.98% and 30.00%, respectively..

The TGA results of the ^{3}L$_2$Co complex show a single-step weight loss over the temperature range of 120–600 °C, corresponding to the loss of $C_{15}H_{20}O_2N_2$. The experimental and theoretical mass losses were both 35.99%.

In summary, thermogravimetric analysis (TGA) shows that the prepared complexes are highly thermally stable, showing very little mass loss even at lower temperatures. This confirms that the complexes contain no traces of solvent. Moreover, the decomposition behavior and the weight losses observed are consistent with the suggested structures.

Table 4: Thermogravimetric (TG) Data of Synthesized Complexes

Complex	Stage	Temperature Range	Found Weight%	Calculated Weight %	Lost Formula
^{1}L$_2$Ru	First stage	120-600	33.47	33.47	$C_{13}H_{17}O$ N Cl
		100-270	8.99	8.99	
^{1}L$_2$Co	First stage				C_3H_7N
	Second stage	270-600	29.98	30	$C_{11}H_{12}O_2N$
^{3}L$_2$Co	First stage	120-600	35.99	35.99	$C_{15}H_{20}O_2N_2$

Anticancer Activity

The anticancer activity of the synthesized chalcone ligand (^{1}L,^{2}L,^{3}L) and its metal complexes (^{1}L$_2$Co, ^{1}L$_2$Ru, ^{2}L$_2$Co,^{2}L$_2$Ru,^{3}L$_2$Co and ^{3}L$_2$Ru) was investigated against lung cancer cells to evaluate their potential cytotoxic effects. Preliminary screening revealed that compounds (^{1}L) and (^{1}L$_2$Co) exhibited inhibitory activity against cancer cells while showing lower toxicity toward normal cells at a concentration of 1 mM, as illustrated in Figure (10). The remaining compounds either showed limited inhibitory activity against cancer cells or exhibited considerable toxicity toward normal cells.

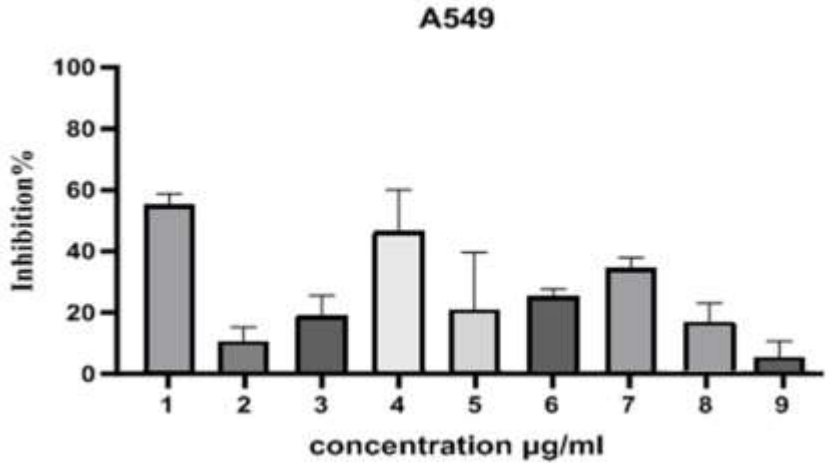


Figure10: Cytotoxic Activity of the Compounds Against Cancer Cells at a Concentration of 1000 µM

Based on the preliminary screening results, compounds (^{1}L) and (^1L_2Co) were selected for further evaluation at three different concentrations against A549 lung cancer cells and HBL-100 normal cells. This investigation aimed to assess their concentration-dependent cytotoxic effects and identify the concentrations associated with effective anticancer activity and lower toxicity toward normal cells. The results are presented in Figures (11,12), while the corresponding IC_{50} values are summarized in Table (5).

The results demonstrated that compounds (^{1}L) and (^1L_2Co) exhibited promising anticancer activity against A549 cells, as indicated by their inhibitory effects and IC_{50} values. Furthermore, their comparatively lower cytotoxicity toward HBL-100 normal cells suggests a degree of selectivity toward cancer cells. The comparison of IC_{50} values between cancerous and normal cells provides an important indication of the potential therapeutic selectivity of these compounds.

Overall, these findings highlight the potential of the selected chalcone derivatives and their metal complexes as promising candidates for further investigation of their anticancer properties. However, additional studies are required to elucidate their mechanisms of action and establish their selectivity and safety profiles.[44–47]

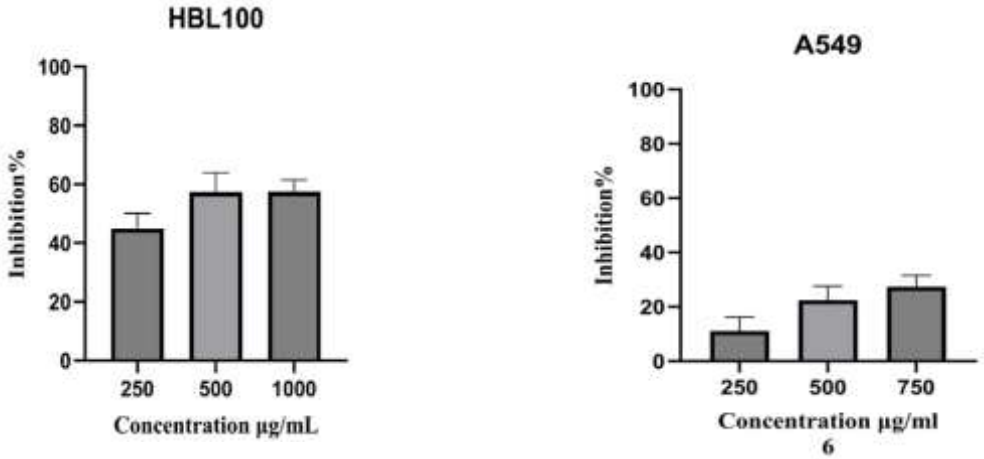


Figure (11). Inhibitory effects of compound ^{1}L on lung cancer cells and normal cells at three different concentrations.

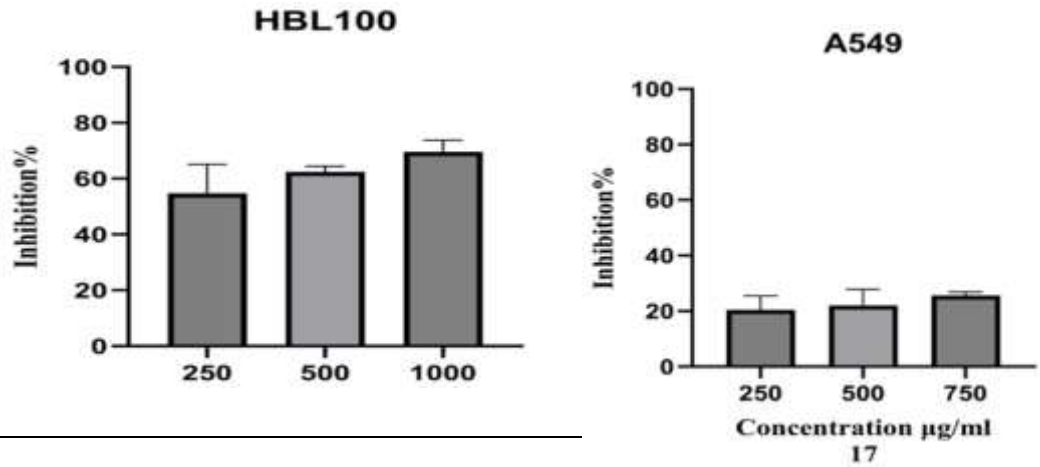


Figure (12). Inhibitory effects of compound (^1L_2Co) on lung cancer cells and normal cells at three different concentrations.

Table (5). IC_{50} values of the tested compounds against lung cancer cells.

Symbol	L	LCo
IC_{50}	776.9	788.2

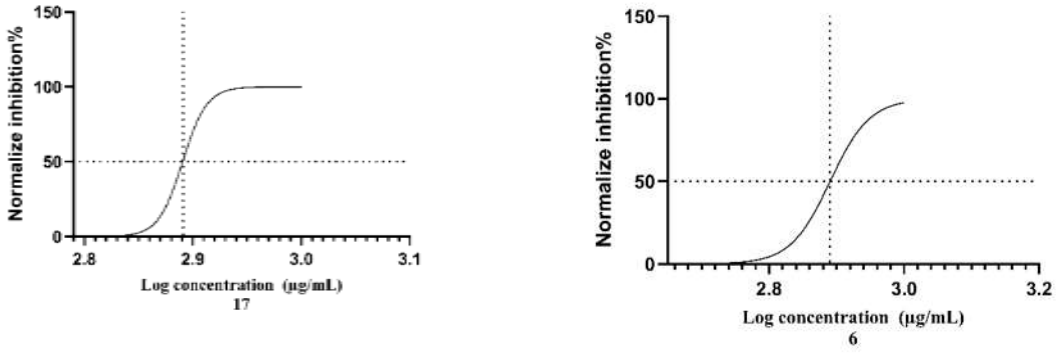


Figure 13. Graphs illustrating the IC_{50} determination for

Molecular Docking Study

Molecular docking was performed to investigate the binding interactions between the compounds that exhibited anticancer activity and the target protein associated with cancer cell proliferation. The protein with PDB ID: 4ASD was selected from the Protein Data Bank (PDB) (4). The three-dimensional structure of the protein was retrieved in PDB format, followed by the removal of water molecules and the addition of polar hydrogen atoms and charges.

Geometry optimization was performed using Gaussian software. The ligand structures were optimized at the APFD/6-311G(d,p) level of theory, while the metal complexes were optimized using the APFD/LANL2DZ level of theory. Molecular docking simulations were carried out using AutoDock 4.2, and the resulting interactions were analyzed and visualized using Discovery Studio.

The docking results revealed variations in binding affinity energies and interaction patterns between the investigated compounds and the amino acid residues of the target protein. The observed interactions included hydrogen bonds and van der Waals forces, which may contribute to the stability of the ligand–protein complexes. Among the investigated compounds, compound ^{1}L exhibited the lowest binding affinity energy, with a value of −9.273 kcal/mol, indicating a potentially favorable interaction with the target protein. The binding affinity energies of the investigated compounds are summarized in Table **(6)**[48, 49] .

Table 6. Binding affinity energies, types of interactions with amino acid residues, and interatomic distances (Å).

Compounds	Interacting Residue	Interaction type	Distance	Binding energy
^{1}L	LYS920	Conventional Hydrogen Bond	2.424	9.273-
	CYS919	Pi-Sulfur	5.8484	
	CYS1045	Pi-Sulfur	4.77064	
	PHE1047	Pi-Pi Stacked	4.39276	
	PHE921	Amide-Pi Stacked	3.8778	
	LEU840	Pi-Alkyl	4.69358	
	VAL848	Pi-Alkyl	5.46599	
	ALA866	Pi-Alkyl	4.1544	
	LEU1035	Pi-Alkyl	4.70069	
	VAL848	Pi-Alkyl	4.57801	
	ALA866	Pi-Alkyl	5.41085	
	VAL916	Pi-Alkyl	5.2626	
	ASP1046	Carbon Hydrogen Bond	3.76325	
	ASP1046	Carbon Hydrogen Bond	3.63861	
	ASP1046	Pi-Anion	4.96278	

^1L_2Co	ILE888	Pi-Sigma	3.98054	-8.93
	LEU1049	Pi-Sigma	3.43967	
	ILE1053	Pi-Sigma	3.51288	
	ARG1027	Pi-Alkyl	4.53487	
	LEU1049	Pi-Alkyl	5.22333	

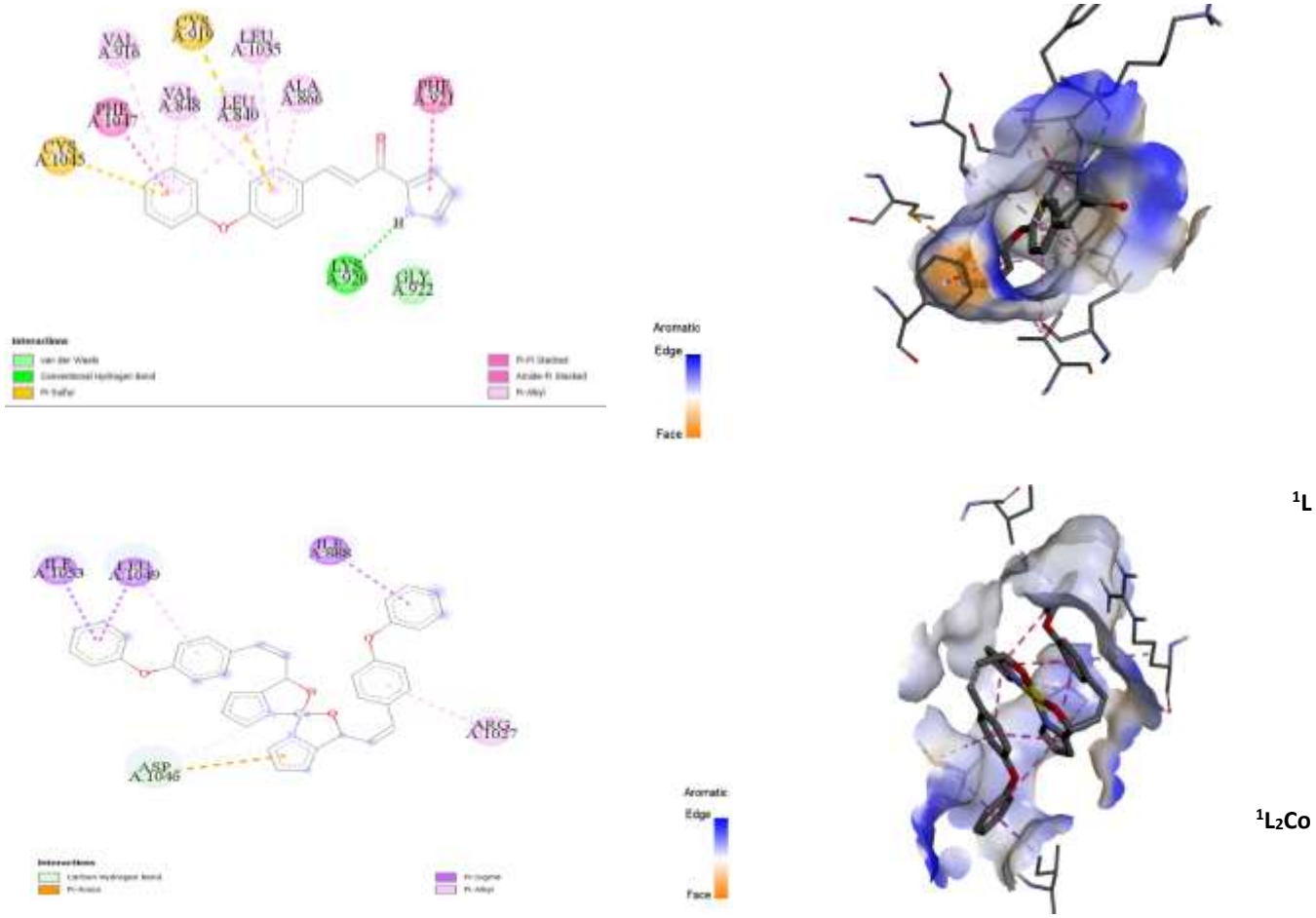


Figure 13. Anticancer activity of the chalcone ligand and its metal complexes

Conclusion:

The successful synthesis of a Chalcone ligand using (3-Phenoxy benzaldehyde) and 2- Acetyl Pyrrole as precursors was carried out in order to synthesize binuclear complexes of Co(II)and Ru(III). The synthesized compounds were characterized using FTIR, 1H NMR, 13C NMR, UV-Vis spectroscopy, mass spectrometry, molar conductivity, magnetic susceptibility, and thermal gravimetric analysis. Based on the analysis, coordination is assumed to occur through the nitrogen atom of the pyrrole ring and Oxygen atom of the carbonyl group of the chalcone ligand, and tetrahedral geometries are proposed for the investigated coordination compounds. The anticancer results show that coordination affects the chalcones biological activity.

Among the investigated compounds, (^1L) and its cobalt(II) complex (^1L_2Co) were evaluated for their anticancer activity against A549 lung cancer cells and their cytotoxic effects on normal HBL-100 cells. Preliminary screening identified compounds (^1L) and (^1L_2Co) as promising candidates, exhibiting inhibitory effects against cancer cells while showing lower toxicity toward normal cells. Further evaluation at three different concentrations revealed their concentration-dependent cytotoxic effects, and the IC_{50} values were determined to assess their potency. Based on the experimental findings, compounds (^1L) and (^1L_2Co) demonstrated promising anticancer activity and comparatively lower cytotoxicity toward normal cells, suggesting potential selectivity toward cancer cells..

This research shows that the anticancer activity of chalcone coordination compounds depends significantly on the type of coordinated metal ion. The cobalt complex shows the highest anticancer activity.

.

Conflict of Interest:
The authors affirm that this work has no conflicts of interest.
Authors' Declaration:
The authors certify that the study described in this publication is wholly original. They take full responsibility for any assertions or problems resulting from the article's content.
Acknowledgements:
The authors extend their sincere appreciation to Dr Sarmad Awad, Faculty of the Department of Biology, College of Education for Pure Sciences, University of Basrah, Iraq, for his valuable assistance in assessing the antibacterial activity of the investigated compounds.

References:

1. Patel, K., et al. (2022). Industrial and environmental applications of transition metal chalcone complexes: A comprehensive review. Applied Organometallic Chemistry, 36(8), e6780. DOI: 10.1002/aoc.6780.
2. Mahmoud, A. M., et al. (2021). Metal-based chalcone complexes: Promising agents for combating therapeutic resistance in tumors. Inorganica Chimica Acta, 520, 120286. DOI: 10.1016/j.ica.2021.120286
3. Abu-Zaied, M. A., et al. (2021). Design, synthesis, and molecular docking of novel chalcone derivatives as potential VEGFR-2 inhibitors and anticancer agents. Bioorganic Chemistry, 114, 105085. DOI: 10.1016/j.bioorg.2021.105085.
4. Karki, R., et al. (2020). Recent progress on chalcones as a potential scaffold for anticancer drug design. European Journal of Medicinal Chemistry, 204, 112613. DOI: 10.1016/j.ejmech.2020.112613.
5.] Gomes, M. N., et al. (2021). Chalcone derivatives: Promising starting points for drug design. Molecules, 26(17), 5319. DOI: 10.3390/molecules26175319.
6. El-Sayed, W. A., et al. (2022). Synthesis, biological evaluation, and molecular docking studies of new chalcone-based metal complexes as targeted anticancer agents. Journal of Molecular Structure, 1254, 132356. DOI: 10.1016/j.molstruc.2022.132356.
7. Kumar, V., et al. (2023). Advances in the development of multi-target directed chalcones for cancer therapy. Drug Discovery Today, 28(4), 103521. DOI: 10.1016/j.drudis.2023.103521.
8. Abdel-Motaal, M., et al. (2023). Novel N-Arylmethyl-aniline/chalcone hybrids as potential VEGFR-2 inhibitors for NSCLC treatment. Journal of Enzyme Inhibition and Medicinal Chemistry, 38(1), 2278022. DOI: 10.1080/14756366.2023.22780229.
9. Zhuang, C., et al. (2020). Chalcone: A Privileged Structure in Medicinal Chemistry. Chemical Reviews, 117(12), 7762–7810. DOI: 10.1021/acs.chemrev.7b00020.
10. Sharma, A., et al. (2022). Transition metal complexes of chalcones: A review of their synthesis and biological activities. Coordination Chemistry Reviews, 452, 214301. DOI: 10.1016/j.ccr.2021.214301.
11. Bao, X., et al. (2022). Structural modifications of the chalcone framework for the development of potent VEGFR-2 inhibitors. Bioorganic & Medicinal Chemistry Letters, 60, 128574. DOI: 10.1016/j.bmcl.2022.128574.
12. Rani, A., et al. (2021). Synthesis, biological evaluation, and molecular docking of novel chalcone-linked pyrazole hybrids as VEGFR-2 kinase inhibitors. Journal of Molecular Structure, 1245, 131012. DOI: 10.1016/j.molstruc.2021.131012.
13. Mazal SM, Alharis RA, Al-Shuhaib ZAM, Hussein KA, Ismael SMH (2026) Pyrazoline-based chalcone derivatives and their Cu(II) complexes: Synthesis, molecular docking study, and anti-cancer evaluation against MCF-7 and A549 cancer cells. Indian Journal of Heterocyclic Chemistry 36:7–15
14. Wang, Y., et al. (2021). Targeting angiogenesis in non-small cell lung cancer: Mechanisms and therapeutic strategies. Frontiers in Oncology, 11, 712957. DOI: 10.3389/fonc.2021.712957.
15. Hassan, A. S., et al. (2022). New chalcone derivatives as targeted therapies for non-small cell lung cancer (NSCLC): Synthesis and in vitro evaluation. European Journal of Medicinal Chemistry Reports, 5, 100054. DOI: 10.1016/j.ejmcr.2022.100054
16.] Singh, P., et al. (2020). Anti-angiogenic potential of chalcones: A comprehensive review of mechanisms and therapeutic implications. Pharmacological Research, 159, 105026. DOI: 10.1016/j.phrs.2020.105026.
17. Orozco, M., et al. (2020). Computational and experimental evaluation of novel chalcones against NSCLC cell lines. Scientific Reports, 10, 14235. DOI: 10.1038/s41598-020-71120-x.
18. Ali, M. A., et al. (2023). Design, synthesis, and biological evaluation of novel chalcone-triazole hybrids as potent VEGFR-2 inhibitors. Journal of Enzyme Inhibition and Medicinal Chemistry, 38(1), 215432. DOI: 10.1080/14756366.2023.2165432.
19. Chen, Z., et al. (2020). Chalcone derivatives as potential anticancer agents targeting VEGFR-2: Synthesis, docking, and molecular dynamics simulations. Molecules, 25(18), 4153. DOI: 10.3390/molecules25184153.
20. Zhao, Y., et al. (2023). The role of VEGFR-2 signaling in tumor microenvironment and therapeutic strategies against lung cancer. Cancer Letters, 554, 216012. DOI: 10.1016/j.canlet.2022.216012.
21. Farooq, S., et al. (2021). Synthesis and molecular docking studies of transition metal complexes of chalcones against angiogenesis targets. Polyhedron, 198, 115065. DOI: 10.1016/j.poly.2021.115065.

22. Popatkar BB, Yadav S, Manjare SB, Borge V V. (2025) Green methods for the synthesis of chalcones: An overview with appraisal to sustainable development and bioactive compounds. Organic Communications 18:38–59
23. Nicolás C, Andrea C, Gustavo S, Marcelo P Ultrasound-assisted syntheses of chalcones: Experimental design and optimization Proceedings, 2019, 41(1), 13. MDPI. https://doi.org/10.3390/ecsoc-23-06475.
24. Saif M. I. Al-Sabawy, Khalid Al-Badrany. (2024). Synthesis and Characterization and Biological Study of Some Cyclohexenone Derivatives from 2-Acetyl Pyrrol. European Journal of Modern Medicine and Practice, 4(7), 321–329.
25. Goel A, Rani M (2023) Synthesis and catalytic activity of Cu (II) complex with 4-phenyl 2, 6-di (thiazol-2-yl) pyridine in the oxidation of para-aminophenol. Current Chemistry Letters 12:193–202
26. Gunasekharan M, Choi TI, Rukayadi Y, Latif MAM, Karunakaran T, Faudzi SMM, Kim CH (2021) Preliminary insight of pyrrolylated-chalcones as new anti-methicillin-resistant staphylococcus aureus (Anti-mrsa) agents. Molecules. https://doi.org/10.3390/molecules26175314
27. Acer J. Hamad, Hamdia H. Jawad, Kadhim A. Aadim. (2026). Synthesis, Characterization, and Biological Potentials of Chalcones Derivatives. Baghdad Science Journal, 23(3), 772–786. https://doi.org/10.21123/2411-7986.5225
28. Al-Husseini ZNO, Alshawi J (2023) Synthesis, characterization and cytotoxic activity study of Mn (II), Co (II), and metal complexes with new schiff base against the hepatocellular carcinoma (SK-GT-4) cancer cell. Onkologia i Radioterapia 17:
29. Hussien NJ, Alshawi JMS, Abdullah KT, Yousif EI, Al Jeboori MJ (2025) Dimethyltin (IV) complexes of new thiosemicarbazone ligand with piperazine1-yimethylene moiety: Synthesis, spectral characterization and antibacterial activity. Edelweiss Applied Science and Technology 9:266–278
30. Yassin, S. K., Ismael, S., Sadia, M., Hussein, K., & Kawkab, A. (2026). Synthesis, characterization, biological activity, and DFT study of some novel Schiff bases. Tropical Journal of Natural Product Research, 10(7), 10728. doi. 10.26538/tjnpr/v10i7.70
31. Jasim M. S. Alshawi, Baidaa K. Al-Rubaye, Hanadi M. Jarallah, Sadiq M.-H. Ismael, Mohamad J. Al-Jeboori, Inigo J. Vitorica-Yrezabal, Richard E. P. Winpenny. (2026). Synthesis, spectroscopic and single-crystal analysis, and DFT studies of N_2O_2 diamine coordination complexes: solvent-driven geometry switching and NLO properties. Inorganic Chemistry Communications, 183, 115873. https://doi.org/10.1016/j.inoche.2025.115873.
32. Susanti Y, Fariati F, Effendy E, Azizah YN (2023) Structure Prediction and Ultrasonic Assisted Synthesis of Coordination Compound Cadmium (II) Bromide with N,N'-diethylthiourea Ligand. Jurnal Kimia Valensi 9:145–154
33. Dermitzaki D, Panagiotopoulou A, Pissas M, Sanakis Y, Psycharis V, Raptopoulou CP (2022) Synthesis, Crystal Structures and Magnetic Properties of Trinuclear {Ni2Ln} (LnIII = Dy, Ho) and {Ni2Y} Complexes with Schiff Base Ligands. Crystals (Basel). https://doi.org/10.3390/cryst12010095
34. Vikas K (2024) Synthesis and characterization of Co (II), Ni (II) and Cu (II) complexes with unsymmetrical tetradentate Schiff base ligand. Res J Chem Environ 28:82–85
35. Abass Hadi M, Kadhim Kareem I (2020) Sciences Synthesis, Characterization and Spectral Studies of a New Azo-Schiff base Ligand Derived from 3,4-diamino benzophenone and its Complexes with Selected Metal Ions.
36. Al-Fakeh MS, Alsikhan MA, Alnawmasi JS (2023) Physico-Chemical Study of Mn(II), Co(II), Cu(II), Cr(III), and Pd(II) Complexes with Schiff-Base and Aminopyrimidyl Derivatives and Anti-Cancer, Antioxidant, Antimicrobial Applications. Molecules. https://doi.org/10.3390/molecules28062555
37. Bale AT, Osunniran WA, Sadiya MH, Adebona FO (2025) FT-IR and UV-Vis Spectroscopic studies of Co(II), Cu(II) and Mn(II) metal complexes of 2-methoxy-2'-hydroxychalcone. International Journal of Research in Pharmacy and Allied Science. https://doi.org/10.71431/ijrpas.2025.4412
38. Al-Kattan WT, Al-Nidaa EM (2014) Synthesis and characterization of Mn(II), Co(II), Ni(II) and Cu(II) complexes with Schiff bases derived from terephthalaldehyde and isophthalaldehyde.
39. Jasim Alshawi, Zainab Salih, & Sara Yassin. (2020). Synthesis, characterization and cytotoxic activity study of Cu (II), Co (II), Mn (II), Ni (II) and Cr (III) Metal Complexes with new guanidine Schiff base against the hepatocellular Carcinoma (HCAM) cancer cell. Egyptian Journal of Chemistry, 63(10). https://doi.org/10.21608/ejchem.2020.37893.2778.
40. Refat MS, Gaber A, Alsanie WF, Kobeasy MI, Zakaria R, Alam K (2021) Utilization and simulation of innovative new binuclear Co(ii), Ni(ii), Cu(ii), and Zn(ii) diimine Schiff base complexes in sterilization and coronavirus resistance (Covid-19). Open Chem 19:772–784
41. Mankhi ZH, Ali HM, Hussain MS (2025) Integrated Thermogravimetric and Spectroscopic Evaluation of Azo Dye and Its Polymers: Focused Analytical Characterization of the Dye and Broad Assessment of Antibacterial Activity. In: Annales de Chimie. Science des Materiaux. International Information and Engineering Technology Association (IIETA), p 145
42. Islam S, Asaduzzaman, Simol HA, Bakshi PK (2024) Synthesis, characterization, and evaluation of the antimicrobial, cytotoxic properties of alkaline earth metal complexes containing the nucleobase guanine. Chemical Papers 78:5545–5561
43. Hussain Al-Daffay RK, Salih Al-Hamdani AA (2022) Synthesis and Characterization of Some Metals Complexes with New Acidicazo Ligand 4-[(2-Amino-4-Phenylazo)-Methyl]-Cyclohexane Carboxylic Acid. Iraqi Journal of Science 63:3264–3275

44. SM. Falih, ST.Al-Saray, AA.Alfaris, A.A.Al-Ali, The synergistic effect of eucalyptus oil and retinoic acid on human esophagus cancer cell line SK GT-4, (2022) , Egypt. J. Med. Hum. Genet, 23 NFG.
45. A.M.Al-Shammari, W.N.Al-Esmaeel, A.A.Al-Ali, A.A. Hassan, AA.Ahmed , Enhancement of oncolytic activity of Newcastle disease virus through combination with retinoic acid against digestive system malignancies, (2019) , Mol. Ther, 27, 126-127.
46. R.I.Freshney, Culture of animal cells: a manual of basic technique and specialized applications, (2010), Wiley-Blackwell, 732.
47. Magda M. F. Ismail, Tamer M. Nasr, Moustafa S.Abusaif, Abeer S.Abdelmoniem & Yousry A.Ammar., Novel niclosamide-derived Schiff bases as a dual-targeted anticancer agents., Scientific Reports | (2026) 16:1959 | https://doi.org/10.1038/s41598-025-33185-2.
48. Hany M.AbdEl-Lateef, Mohammed A. I. Elbastawesy , Tamer Mohamed Abdelghani Ibrahim, Mai M.Khalaf, MohamedGouda, Mariam G. F. Wahba, Islam Zaki and MarthaM.Morcoss., Design, Synthesis, Docking Study, and Antiproliferative Evaluation of Novel Schiff Base–Benzimidazole Hybrids with VEGFR-2 Inhibitory Activity., Molecules 2023, 28(2), 481; https://doi.org/10.3390/molecules28020481
49. Haider J. Al-Karagully and Mohammed Kamil Hadi, Molecular Docking, ADMET Study, Synthesis, Characterization, and Antiproliferative Activity Study of Novel Schiff Base Derivatives of N'- benzylidene-4H-benzo[b][1,4]thiazine-3-carbohydrazide Against Lung Cancer Cell Line. Iraqi J Pharm Sci, Vol.35(1) 2026 DOI: https://doi.org/10.31351/vol35iss1pp98-111